nature water

Analysis

https://doi.org/10.1038/s44221-026-00619-8

Coastal groundwater-level trends reveal global susceptibility to seawater intrusion

Received: 19 August 2025

Accepted: 5 March 2026

Published online: 14 April 2026

Check for updates

Annika Nolte[1,2] ✉, Steffen Bender[2], Jens Hartmann[1], Stefan Baltruschat[1], Nils Moosdorf[3,4] & Robert Reinecke[5]

Coastal groundwater is a vital freshwater source threatened by overabstraction and sea-level rise, yet global patterns of declining groundwater levels and susceptibility to seawater intrusion (SWI) remain poorly constrained. Here we present a global assessment based on in situ observations from ~480,000 coastal monitoring locations. From 1990 to 2024, 21% of gridded coastal areas show statistically detectable rising or falling groundwater-level trends with magnitudes ≥0.1 m yr^{-1} and with declines becoming more frequent in the last 9 years. More pronounced changes are observed for deeper water tables ($\rho_s = 0.63$), in arid settings ($\rho_s = 0.56$) and in some rural areas. Seawater intrusion susceptibility is higher where seaward freshwater discharge is weak or where hydraulic gradients reverse landward, leaving limited hydraulic resistance to seawater intrusion. Extrapolating observed trends suggests that these conditions mostly persist (93.4%), while 3.5% newly emerge and 3.1% stabilize (gradients strengthen seaward). The results provide global evidence for prioritizing monitoring and management of coastal groundwater at risk of salinization.

Groundwater is a critical freshwater source in coastal regions, which are home to 2.86 billion people[1], and plays a vital role in sustaining coastal ecosystems and their services[2,3] as well as marine biota[4]. However, coastal aquifers face pressure from growing coastal populations[5], and are increasingly vulnerable to seawater intrusion (SWI), which threatens both the quantity and quality of available water. Salinization reduces water suitability for human use. It has adverse health impacts when drinking-water salinity increases[6], threatens agriculture by lowering soil fertility and crop yields when salinity of irrigation water increases[7], and affects coastal ecosystems, where increased salinity can stress vegetation and soil communities and lead to shifts in species composition[8,9]. Climate change and, as a consequence, sea-level rise, changes in groundwater recharge and intensifying water use increase pressure on coastal groundwater systems[10–12]. This makes it increasingly important to identify where coastal groundwater resources are susceptible to SWI and where monitoring and management should focus to detect and respond to emerging threats.

In coastal settings, hydraulic gradients at the land–sea boundary govern the balance between fresh submarine groundwater discharge and the intrusion of seawater into the nearshore aquifer. Persistent landward or near-zero seaward gradients therefore favour lateral SWI and constitute a first-order control on coastal groundwater–ocean exchange[13–15]. Here we use the hydraulic gradient as a scalable proxy for whether freshwater tends to discharge seaward or seawater tends to intrude landward. Gradients summarize coastal head differences and thus integrate the effects of multiple controls. Aquifer properties and architecture, including surface-water connectivity, modulate how natural recharge, human pressures (for example, groundwater abstraction, land drainage and land-surface changes that modify recharge) and sea-level rise translate into gradients[13]. In particular, two natural settings predispose coasts to landward or near-zero seaward gradients by constraining freshwater heads: topography-limited low-relief coastal plains and recharge-limited (often arid and water-limited) settings[16]. In topography-limited settings, freshwater heads are already close to the land surface, leaving limited capacity for further head increase under sea-level rise. In recharge-limited settings, limited replenishment suppresses freshwater heads and constrains head recovery.

[1]Institute for Geology, Universität Hamburg, Hamburg, Germany. [2]Climate Service Center Germany (GERICS), Helmholtz-Zentrum Hereon, Hamburg, Germany. [3]Leibniz Centre for Tropical Marine Research (ZMT), Bremen, Germany. [4]Institute of Geosciences, Kiel University, Kiel, Germany. [5]Institute of Geography, Johannes Gutenberg University Mainz, Mainz, Germany. ✉e-mail: annika.nolte@posteo.de

Here long groundwater response times (hydraulic memory) can delay and buffer responses to climate variability, even as water-table sensitivity to recharge or precipitation can be high and increase with aridity[17,18]. Projected aridification and shifting precipitation regimes are expected to further reduce recharge in recharge-limited coasts, increasing SWI susceptibility[11].

Yet despite our general process understanding, the global spatiotemporal distribution of SWI-susceptible conditions remains poorly characterized. This limits our ability to anticipate where and how salinization pressures may intensify under future climatic and anthropogenic change and reflects broader limitations in global groundwater assessments, which often lack the resolution, integration and observational grounding needed to capture the complexity of groundwater systems[19]. Most assessments of coastal groundwater systems are focused on local or regional case studies (for example, refs. 20,21), which presents challenges of commensurability when seeking a better understanding about global-scale processes[22]. Global approaches to model SWI[23–25] continue to face high uncertainties due to assumptions concerning boundary conditions and hydrogeological parameterization, and are challenging to evaluate because of the coarse spatial resolution and spatially biased availability of time-varying groundwater-level (GWL) data[22,26]. GRACE (gravity recovery and climate experiment) satellite observations provide valuable information for major groundwater basins. However, coarse spatial resolution, land–ocean leakage near coasts and the residual-based derivation of groundwater storage changes from model-partitioned water components can yield physically implausible estimates and limit applicability, particularly for smaller or coastal systems[27–29].

In contrast, key indicators of coastal groundwater susceptibility to SWI can be derived from in situ GWL observations, specifically hydraulic heads that favour lateral SWI and declining GWLs that lower freshwater heads[24,30,31]. However, GWLs remain difficult to integrate at scale because of fragmented responsibilities, limited digitization, accessibility issues and non-standardized datasets[32–34]. Despite these challenges, few efforts have leveraged large-sample in situ GWL data. GWL observations globally were compiled by ref. 35. This was the basis for developing modelled estimates of water table depth (WTD) with global coverage (for example, refs. 35,36), now widely used in groundwater-related environmental studies (for example, ref. 37). Recent in situ syntheses have quantified GWL trends across terrestrial aquifer systems globally[38] and regionally in southwestern Europe[39], but without a specific coastal focus. By contrast, ref. 31 focused on coastal areas but limited analysis to the contiguous USA, while ref. 40 used thousands of globally distributed coastal GWL time series to identify common GWL dynamics and highlight limitations of global datasets in explaining these patterns, without deriving GWL trends or explicitly assessing susceptibility to SWI. Collectively, these studies underscore both the value of in situ GWL data and the persistent gap in globally integrated, observation-based assessments of coastal aquifers. Here we compile an unprecedentedly large and diverse global set of in situ coastal GWL observations to derive land–sea hydraulic gradients and recent trends summarized on a common spatial grid for global mapping as observation-based indicators of SWI susceptibility, and to examine how these indicators vary across aridity conditions and coastal regions worldwide.

Susceptible hydroclimatic conditions

Hydroclimatic susceptibility to lateral SWI in our framework is defined by two variables: the land–sea hydraulic gradient that we use as an observation-accessible screening diagnostic and aridity as a practical proxy for natural recharge limitation. We quantify the land–sea gradient as the change in hydraulic head between inland monitoring locations and the coastline, divided by their distance to the coastline, and classify it as 'flat' when it is landward or weakly seaward ($\leq 10^{-3}$ m m^{-1}). This 'flat-gradient' class favours lateral SWI[24,30]. All remaining gradients are grouped as steep ($>10^{-3}$), representing stronger seaward head gradients that generally oppose inland SWI. While this steep class spans a wide range of seaward conditions, we use this binary split as a simple, transparent global screening. Aridity is represented by the aridity index (AI; the ratio of precipitation to potential evapotranspiration[41]), with water-limited climates (AI ≤ 1; rather dry) contrasted against energy-limited climates (AI > 1; rather wet). The combination of flat gradients and water-limited climates forms the most susceptible hydroclimatic cluster (C1) in our analysis (Fig. 1; Methods). WTD provides important context because shallow groundwater implies limited vadose storage, so modest declines can more readily weaken land–sea gradients and increase salinization risk. Globally, aquifers near coasts are often shallow: the median coastal WTD is 6.1 m and nearly half of all observations are shallower than 5 m (Supplementary Information Section A). Flat gradients, which weaken the natural flow of groundwater towards the sea, are found in about one-third of all observed coastal areas. Although steeper gradients dominate overall (skewed distribution in Fig. 1a), flat gradients remain common even tens of kilometres inland (34–37% of all observations; Fig. 1c). Compared with the global aridity distribution of coastal regions, our dataset shows a distinct clustering near the transitional AI value of approximately 1 (marking the boundary between water- and energy-limited climates), a zone in which groundwater recharge is expected to be particularly sensitive to modest shifts in long-term aridity[42]. In contrast, moderately arid regions (AI ≈ 0.3–0.7) and humid regions (AI > 1) are under-represented in our dataset (Fig. 1b). Overall, 74% of observations fall within water-limited environments (AI ≤ 1). Importantly, flat-gradient, water-limited conditions (C1; most susceptible) are most frequent within 1 km of the coastline, where they account for 28% of observations, but they also occur further inland (Fig. 1c). In Fig. 1d, C1 forms contiguous coastal belts in IPCC reference regions[43] such as the southeastern USA (ENA), Gulf of Mexico (CNA and SCA) and northeast Australia (parts of CAU and NAU). Steep-gradient, water-limited conditions (C2) dominate across all coastal distances (Fig. 1c). Near the coast, C2 accounts for 52% of observations. By contrast, susceptibility conditions, where gradients are flat but recharge is not limiting (C3), are least common.

Prevalence of trends and sensitivity to record length

Changes in GWLs alter freshwater heads and, therefore, the land–sea hydraulic gradients. For the 34-year period 1990–2024 studied, our trend analyses show that 28% of observations exhibit statistically significant GWL changes exceeding ±0.1 m yr^{-1} over 9-year windows. A total 21% of observations exhibit such trends when evaluated over 19-year windows. The frequency of upward and downward changes in GWLs is balanced across both periods, with a slight bias towards declines in the shorter timeframe (42% upward compared with 58% downward among absolute trends). To evaluate how strongly record length affects inferred trends, we compared slopes from overlapping 9- and 19-year windows for the subset of observations with both time frames available (Supplementary Information Sections B2 and B3). These are moderately correlated across windows (Spearman $\rho_s = 0.58$). Trend direction is consistent in most observations (76%), while ~19% are ambiguous. Here the 9- and 19-year slopes have opposite signs, but at least one slope is near zero (|slope| < 0.1 m yr^{-1}), so the apparent sign switch mainly reflects near-stable conditions in one window rather than a clear reversal. Only ~5% show clearly inconsistent opposite-sign trends with |slope| ≥ 0.1 m yr^{-1} in both time windows. Agreement is similar at the scale of Intergovernmental Panel on Climate Change (IPCC) regions ($\rho_s = 0.58$; 78% consistent), although a few regions exhibit sign changes in median trends (notably EAU, as well as NCA, SAS and MDG in Fig. 2). Large trend magnitudes (that is, strongly upward or strongly downward trends, |slope| > 0.5 m yr^{-1}) occur less frequently over 19-year windows than over 9-year windows. This is consistent with longer records integrating low-frequency variability and episodic events[44,45].

https://doi.org/10.1038/s44221-026-00619-8

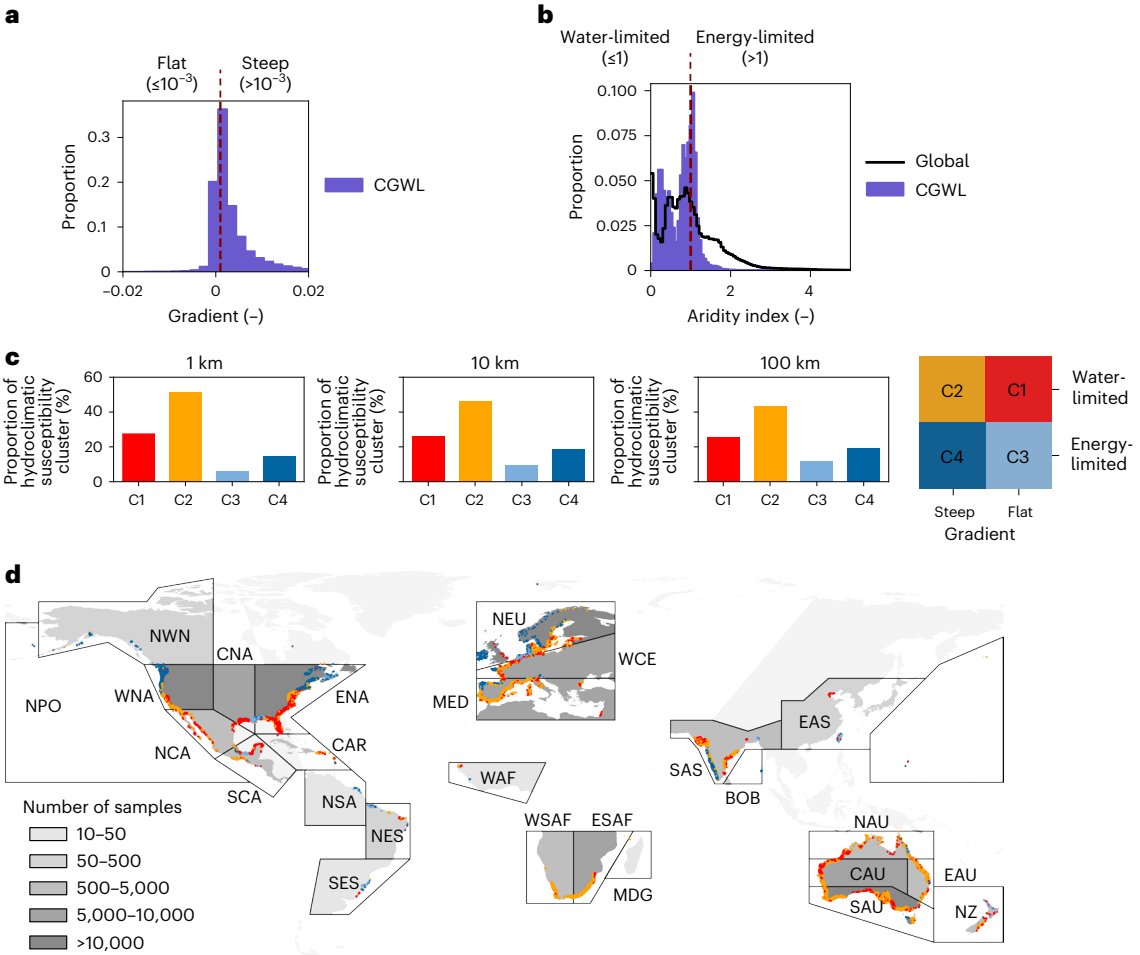

Fig. 1 | Global hydroclimatic patterns indicating susceptibility of coastal groundwater systems to SWI. Global patterns of hydroclimatic conditions indicating susceptibility of coastal groundwater systems to SWI. **a**, Distribution of land–sea hydraulic gradients derived from the CGWL dataset, with a red dashed line marking the threshold separating flat (≤10^{-3}; landward or near-zero seaward gradients) from steep seaward gradients. **b**, Distribution of AI values[41,60] for the CGWL dataset and coastal regions globally, with a red dashed line marking the climatic threshold (AI ≈ 1) used to distinguish water- and energy-limited regimes. **c**, Proportions of four hydroclimatic susceptibility clusters (C1–C4) at three distances from the coastline (1 km, 10 km and 100 km). **d**, Global distribution of categorized observations (plotted in grid-cell centres with random overlap of clusters), shown together with the number of samples in IPCC reference regions[43] with ≥10 observations. Land and coastline geometry in **d** from HydroBASINS[64,65]. IPCC reference region geometries in **d** from refs. 43,75.

For subsequent analyses, we use a combined trend product, assigning 19-year trends where available and otherwise using 9-year trends. Globally, 24% of observations show significant GWL trends, of which 54% are downward. GWL changes are mapped with their magnitude and direction in Fig. 2. The prevalence of declining and rising GWLs varies spatially, ranging from under 10% (for example, northern Europe—NEU) to over 40% (for example, South Africa—WSAF and ESAF; North and Central America—WNA, CAN and NCA). Individual observations reveal strong within-region variability, with localized clusters of opposing trend directions and magnitudes.

Trends in rural and urban coastal regions

Urban and rural areas often differ in land use and water management, which can influence groundwater dynamics. We therefore stratify the dataset by a rural–urban typology[46]. Figure 2 reveals rural–urban differences in GWL changes. Overall, rural areas show a slightly higher prevalence of significant GWL trends (|slope| ≥ 0.1 m yr^{-1}) than urban areas and the trend magnitude is weakly negatively correlated with population density (ρ_s: −0.17). This global rural–urban contrast is driven mainly by specific regions, including India (SAS), northern Central America (NCA), Australia (SAU, EAU and NAU) and New Zealand (NZ). Urban observations show more frequent trends in fewer regions, especially southern Central America (SCA), central North America around the Gulf of Mexico (CAN) and eastern South Africa (WSAF). Overall, these regional differences sum to a higher global prevalence of significant trends in rural than urban areas (26% versus 22%), with declines accounting for ~54% and ~55% of observations with trends, respectively.

Identifying hotspots of SWI susceptibility

To link hydroclimatic susceptibility from aridity and land–sea hydraulic gradients (clusters C1–C4) with dynamic change, we examine how GWL trends vary across clusters and coastal distances. First, we quantify pairwise relationships using Spearman correlations between absolute trend magnitude (|slope|) and aridity, WTD and hydraulic gradient. These correlations are stronger inland than near the coast. At 100 km from the coastline, the trend magnitude correlates with drier conditions (ρ_s = 0.56), with deeper water tables (ρ_s = 0.63) and with larger land–sea hydraulic gradients (ρ_s = 0.36). Aridity and WTD co-vary (ρ_s = 0.50), indicating that drier conditions tend to coincide with deeper water tables. At 1 km from the coast, associations weaken but remain detectable for aridity and WTD (ρ_s = 0.19 and ρ_s = 0.41), whereas the association with hydraulic gradient is negligible. Second, consistent with these pairwise patterns, trend frequencies differ across susceptibility clusters (Fig. 3). Water-limited clusters (C1 and C2), which often coincide with deeper water tables in arid regions, show the highest frequencies of both

https://doi.org/10.1038/s44221-026-00619-8

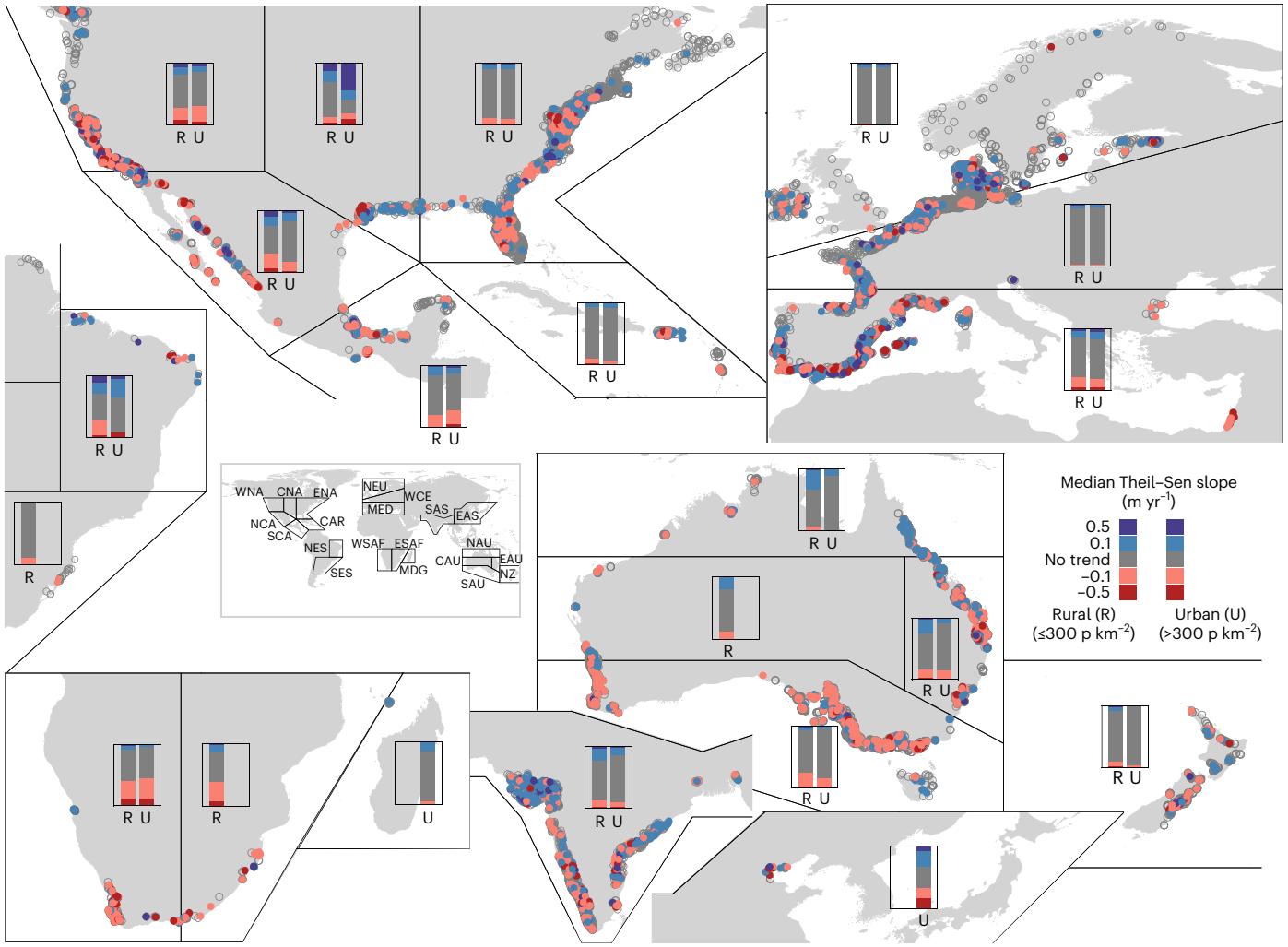

Fig. 2 | Recent groundwater level trends across global coastal zones by IPCC region. Spatial patterns of recent groundwater level trends across global coastal zones, grouped by IPCC reference regions[43]. Coloured points on maps represent individual observations that are plotted in grid-cell centres with random overlap of Theil–Sen slope trend categories on top of 'no trend': strong decline (<−0.5 m yr^{-1}, dark red), moderate decline (−0.5 m yr^{-1} to −0.1 m yr^{-1}, light red), no trend (−0.1 m yr^{-1} to 0.1 m yr^{-1} and/or non-significant, grey), moderate rise (0.1 m yr^{-1} to 0.5 m yr^{-1}, light blue) and strong rise (>0.5 m yr^{-1}, dark blue). Bar charts show the proportions of trend categories per region (≥10 observations), stratified by rural (R; ≤300 people km^{-2}) and urban (U; >300 people km^{-2}) areas[63]. Supporting regional trend results are provided in Supplementary Information Section B5. Land and coastline geometry from HydroBASINS[64,65]. IPCC reference region geometries from refs. 43,75.

upward and downward trends across all coastal distances (absolute trends: 36% and 34%). Although less susceptible in our gradient-aridity screening because of steep gradients, C2 shows the highest prevalence of GWL declines that are most pronounced further inland. Conversely, overall trend activity is much lower in energy-limited clusters (C3 and C4; 3% and 12%). Near the coast, susceptibility and change coincide most strongly: within 1 km, 28% of C1 observations show significant trends, with marginally more GWL declines than rises.

Most trend slopes are moderate (|slope| < 0.5 m yr^{-1}), yet even modest head changes can shift land–sea gradients towards or away from flat-gradient conditions. We therefore used derived GWL trends to extrapolate whether observations may enter, remain in or exit the flat-gradient susceptibility clusters (C1/C3) over the next decade (Fig. 4a). Persistent gradient-based hotspots (93.4% of all sites) are locations already exhibiting SWI-susceptible conditions that are projected to remain within C1 or C3 over the next decade. A smaller fraction (3.1%) is projected to stabilize, meaning that they may transition out of C1/C3 if recent upward trends continue and 3.5% are emerging hotspots, that is, locations projected to transition into flat-gradient conditions (C1/C3) over the next decade.

Discussion

The results of this study are based on deriving physically motivated indicators of SWI susceptibility from integrated in situ GWL observations. Our hydroclimatic susceptibility framework links land–sea hydraulic gradients with aridity conditions and incorporates recent GWL changes to assess how susceptibility states may evolve, even when detailed hydrogeological information is limited. It methodologically extends elevation-based screening approaches[31] and complements previous large-scale GWL trend syntheses (for example, refs. 38,39) by focusing explicitly on coastal aquifer settings. In the USA, coastal regions that we classify as hydroclimatically susceptible show strong spatial concordance with areas highlighted by ref. 31: within 10 km of the coastline, 20% of our observations have groundwater elevations below sea level (versus 27% of wells in ref. 31) and 37% have flat gradients (≤10^{-3}). Globally, our flat-gradient, water-limited cluster (C1) captures major regions with documented SWI compiled in ref. 47 (Fig. 3 in this publication) and ref. 13 (Fig. 1 in this publication). These include the southeastern coasts of the USA, Central America, the Mediterranean, the Cape Town area of South Africa, parts of India and southeastern Australia, which also show a higher prevalence of downward GWL trends in our analysis. Beyond these

https://doi.org/10.1038/s44221-026-00619-8

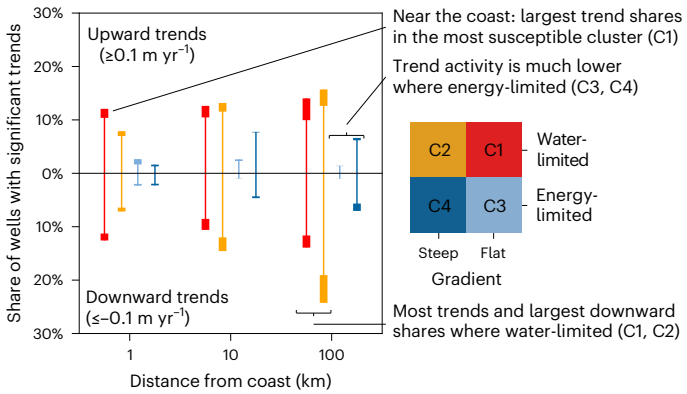

Fig. 3 | Shares of significant groundwater level trends by distance from the coast and SWI susceptibility. Share of wells with significant upward (top, ≥0.1 m yr^{-1}) and downward (bottom, ≤−0.1 m yr^{-1}) trends as a function of distance from the coast (1 km, 10 km and 100 km). Thicker bar segments at the top and bottom indicate the shares of strongly rising (>0.5 m yr^{-1}) and strongly declining (<−0.5 m yr^{-1}) observations, respectively. Differently coloured shares refer to the SWI susceptibility clusters (C1–C4).

documented hotspots, our gradient-aridity framework maps the global extent and relative frequency of comparable hydroclimatic configurations, providing a quantitative screening to guide where monitoring and management could be prioritized. This also helps to mitigate the urban bias noted in ref. 13 because our analysis draws on routine monitoring observations across both urban and rural settings, whereas published SWI case studies are disproportionately from urban, economically developed regions[13]. At the same time, the availability of GWL observations in our analysis shows a heterogenic spatial distribution globally. Coverage is strongest in temperate regions such as Europe and the USA, whereas most of Africa, equatorial regions, large parts of South America and Asia and many small islands remain sparsely represented or are completely missing. Accordingly, several SWI sites reported in Asia, Africa and South America[13,47] fall outside our analysed dataset. Our SWI-susceptibility patterns therefore reflect the spatial footprint of available observations and the absence of mapped hotspots in data-poor regions should not be interpreted as the absence of SWI susceptibility.

This study further shows that continued GWL change can generate SWI-relevant gradients within a single decade and that GWLs near the coastline tend to change most strongly where flat hydraulic gradients coincide with water-limited conditions (C1; most susceptible). While our observation-based indicators do not quantify volumetric freshwater losses, even small deviations and variations around the gradient threshold may become critical over longer timescales. Rising GWLs are as frequent as declines, both globally and often regionally. Coastal aquifers are therefore not uniformly moving towards greater SWI susceptibility. Instead, susceptibility can strengthen or weaken locally, and short-term variability in GWLs, even without sustained declines, can temporarily shift systems towards flat-gradient, SWI-prone conditions. This spatial and temporal variability highlights the value of sustained GWL observations for locally grounded detection of SWI-susceptible conditions.

Further increases in the marine boundary head are likely to shift additional coastlines into SWI-susceptible gradient states[23,25]: The global mean sea level is currently rising at ~4.5 mm yr^{-1} (ref. 48), and is projected to rise by roughly 0.3–1.0 m by 2100 (relative to 1995–2014, depending on emissions scenario), with possible multi-metre rise on longer timescales as peak warming increases[49]. This situation can be further exacerbated by pumping-induced upconing, which can cause SWI even further inland[50]. This matters because our study shows that deep aquifers in rural, arid regions exhibit more widespread declines. Because these systems often respond slowly, management interventions may take years to decades to translate into measurable head recovery, so expectations for SWI susceptibility and monitoring strategies need to account for delayed results. Furthermore, the spatial distribution of significant GWL changes does not align with population density. This should be read as an observed GWL signal, not a direct proxy for local groundwater use, because urban demand is partly met by pumping outside cities. However, our results align with ref. 38, which reports widespread declines in dryland aquifers, particularly under croplands. Hence, groundwater-dependent agricultural regions may face disproportionate SWI susceptibility where high extraction pressures coincide with limited regulatory oversight. Persistent or emerging flat-gradient patterns in our study frequently co-occur with regions where sectoral groundwater withdrawals are already high (Fig. 4c), with agriculture as the dominant groundwater user and increasing withdrawals in many regions since 2001[51]. Beyond SWI, some coastal regions with relatively low gradient-based susceptibility, such as parts of South Africa, show substantial GWL declines together with projected groundwater recharge reductions (Fig. 4b), indicating emerging groundwater-stress risks that are highly relevant in the context of 'day zero' drought-driven water-scarcity crises, where prolonged hydroclimatic deficits and high demand can push water systems into acute supply shortfalls[52]. In such situations, groundwater can be considered a fallback supply[53], but in coastal settings where our indicators suggest SWI susceptibility and/or declining GWLs, this option may be constrained by limited availability.

Conclusions

This study provides a global observation-based assessment of hydroclimatic conditions associated with SWI susceptibility in coastal groundwater systems that is based on in situ GWL observations from ~480,000 coastal monitoring locations. By combining land–sea hydraulic gradients, aridity and recent GWL trends in a bottom-up approach that captures spatiotemporal signals often missed by static frameworks and/or coarse top-down approaches, the study delivers three main contributions. First, it translates the available monitoring footprint into globally comparable quantities that can inform large-scale assessments and reporting (for example, by international frameworks). Second, the study maps where potentially susceptible conditions occur and where they are changing, helping prioritize monitoring and management in coastal regions where risk may be shifting in real time. Third, it provides observation-based indicators that can be systematically incorporated into SWI risk assessments and used as constraints to evaluate and improve large-scale models that simulate unmonitored coasts. At the same time, the hydroclimatic susceptibility indicators do not by themselves resolve local vulnerability or control–response relationships. Doing so requires more detailed hydrogeologic characterization, co-located salinity monitoring and improved global datasets of key controls, alongside broader efforts to expand and strengthen groundwater observations, particularly in regions with large observational gaps. Avoiding or reducing SWI in susceptible settings is critical because salinization of groundwater threatens safe drinking-water supplies, lowers agricultural productivity and degrades coastal and nearshore ecosystems. Looking ahead, our findings highlight that stronger monitoring and data-synthesis efforts can enable scalable, observation-based tools to detect emerging SWI risk early, improve system understanding and inform timely adaptation. Such advances are increasingly important as projected shifts in groundwater recharge, continued sea-level rise and anthropogenic pressures interact with existing flat-gradient settings in many coastal regions.

Methods

We used the coastal groundwater level (CGWL) dataset, a newly compiled global resource of in situ coastal GWL observations from governmental monitoring networks and public portals (Supplementary Information Section A). The CGWL dataset comprises ~629,000 well records (~480,000 unique locations at three-decimal coordinates)

https://doi.org/10.1038/s44221-026-00619-8

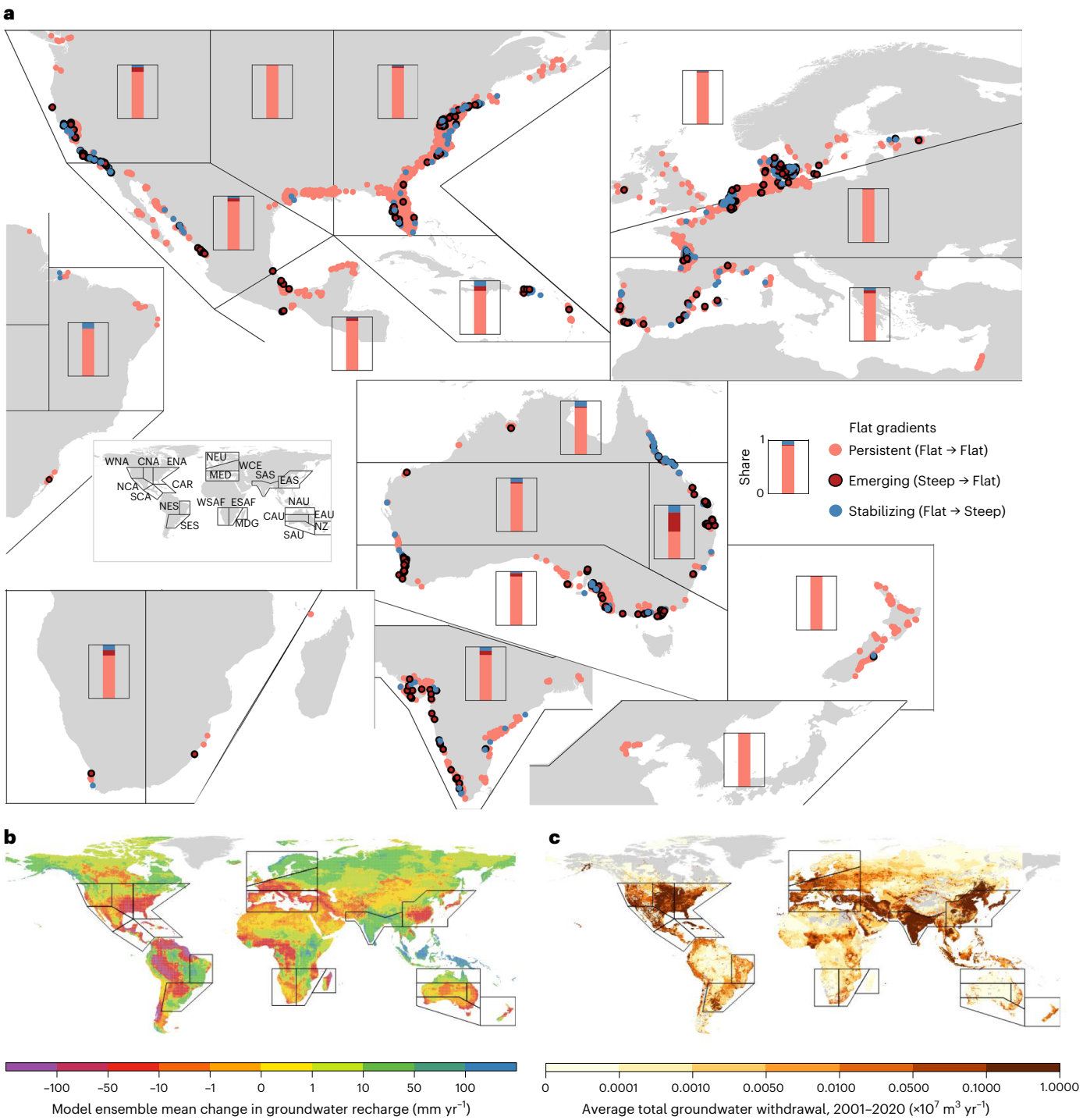

Fig. 4 | Global hotspots of SWI susceptibility and changes in recharge and groundwater withdrawals. a, Spatial patterns of hydroclimatic, gradient-based SWI-susceptibility hotspots across IPCC regions[43], derived from trend extrapolation. Points show individual observations (grid-cell centres). Hotspots are defined relative to the flat-gradient clusters C1/C3. When colocated, emerging (entering C1/C3 within 10 years) and stabilizing (exiting C1/C3 within 10 years) hotspots are randomly overlaid on persistent hotspots (in C1/C3 now and in 10 years). Bar charts show the relative proportions of hotspot types within each region (≥10 observations). **b**, Model-ensemble mean change in groundwater recharge (mm yr^{-1}) between present-day warming (~1 °C) and 3 °C global warming, from the ISIMIP2b multimodel ensemble[62]. **c**, Long-term mean total groundwater withdrawal (2001–2020; $\times 10^7$ m^3 yr^{-1}), from the data-driven global groundwater withdrawal model[51,61]. Land and coastline geometry in **a**–**c** from HydroBASINS[64,65]. IPCC reference region in **a**–**c** from refs. 43,75.

from wells within 100 km of the coastline and with WTDs shallower than 100 m (Supplementary Information Section A1). Raw groundwater data were quality controlled and harmonized to consistent groundwater depth (WTD; ground-surface reference) and groundwater elevation, using source-provided elevations where available and otherwise CoastalDEM[54] or SRTM[55]. We aggregated groundwater information to hexagonal grid cells with a mean cell area of 0.74 km^2 (H3-8; ref. 56) and refer to these grid-cell aggregates as 'observations'.

Groundwater hydraulic gradients

Land–sea hydraulic gradients were calculated at the grid level using median groundwater elevation and the median Euclidean distance

of wells in the cell to the coastline (dataset[57]). Using medians reduces sensitivity to outliers but also smooths short-term extremes in the hydraulic head that can be relevant for SWI. Because this proxy does not resolve time-varying coastal boundary heads, nonlinear flow paths or within-cell hydrogeologic heterogeneity, gradients may be biased high or low at individual locations. We therefore interpreted them as a first-order, observation-based screening diagnostic of prevailing coastal head conditions. The sample size for gradient analysis comprised 232,419 grid cells with available groundwater elevation and coastline distance data.

Trend analysis

To quantify recent GWL change, we filtered monthly CGWL time series and computed monotonic trends over 9- and 19-year windows within 1990–2024. The record lengths used for the trend analysis were chosen iteratively to balance temporal robustness against global support, consistent with prior large-scale groundwater trend studies[38]. A detailed discussion of window-length trade-offs is provided in the Supplementary Information Section B3. Time-series selection further allowed variable sampling while limiting seasonal distortion (Supplementary Information Section B1). This yielded 51,263 unique monitoring locations with sufficient data to estimate a 9-year trend. Of these, 20,857 locations also met the minimum length for a 19-year trend. Where both are available, the 9-year window corresponds to the final 9 years of the 19-year window. Monotonic trends in GWLs were calculated using the non-parametric modified Mann–Kendall test[58] and corresponding trend magnitudes were estimated using Sen's slope[59]. Trends were computed at the well level and subsequently aggregated to H3-8 grid cells by taking the median of slope values, regardless of individual statistical significance ($P > 0.05$); however, significance flags were retained to support additional filtering. Trend slopes were classified into five trend categories: strongly downward (<−0.5 m yr^{-1}), moderately downward (−0.5 m yr^{-1} to −0.1 m yr^{-1}), no trend (between −0.1 m yr^{-1} and 0.1 m yr^{-1} and/or non-significant), moderately upward (0.1 m yr^{-1} to 0.5 m yr^{-1}) and strongly upward (>0.5 m yr^{-1}). Only a small fraction of results classified as 'no trend' are non-significant solely as a result of statistical insignificance (5.6% for 9-year trends and 1.7% for 19-year trends). After aggregation, trend results were available for 36,579 grid cells (9-year) and 17,703 grid cells (19-year), so that 19-year trends support ~41% of grid-level trend estimates globally (Supplementary Information Section B2).

Hydroclimatic classification and hotspot extrapolation

Hydroclimatic susceptibility was applied along two axes: aridity (as a proxy for recharge limitation) and land–sea hydraulic gradient (as a proxy for the tendency towards seaward discharge versus inland salinity advance). To classify gradients, we used two categories based on model-informed thresholds: flat (≤10^{-3}, landward or near-zero seaward gradients) and steep seaward gradients (>10^{-3}), following refs. 24,30, showing that gradients lower than 10^{-3} are more prone to SWI or to the persistence of saline groundwater. Each H3-8 grid cell was further assigned the AI[41,60], which represents the ratio of precipitation to potential evapotranspiration. Cells were categorized as either water-limited (AI ≤ 1) or energy-limited (AI > 1). These binary classes define clusters C1–C4 used throughout this study:

- C1 (most susceptible): flat gradient (≤10^{-3}) and water-limited (AI ≤ 1)
- C2: steep gradient (>10^{-3}) and water-limited (AI ≤ 1)
- C3: flat gradient (≤10^{-3}) and energy-limited (AI > 1)
- C4 (least susceptible): steep gradient (>10^{-3}) and energy-limited (AI > 1)

To analyse potential hotspot persistence/emergence under continued change, we extrapolated groundwater elevation using the estimated trend slope over a 10-year horizon, recomputed the projected gradient and evaluated whether grid cells would remain in, enter or exit flat-gradient conditions (C1/C3). This provides a straightforward diagnostic that does not account for potential nonlinearities in drivers of GWL trends or management responses.

Preparing secondary datasets for contextual analyses

The global AI is used directly in the SWI-susceptibility classification. All other secondary datasets were compiled only to contextualize and interpret gradients and GWL trends. Specifically, Fig. 4b,c shows gridded sectoral groundwater withdrawals[51,61] and a multimodel ensemble of groundwater recharge change[62] for visual comparison with our results. We prepared the population density of the year 2020[63] to derive rural–urban classes following Eurostat[46]. This dataset was preprocessed in ArcGIS Pro where information was derived for H3-8 grid cells using zonal statistics.

Limitations

Spatial aggregation framework. We adopted the regular, globally near-equal-area H3-8 grid[56] as a transparent, assumption-light spatial unit that provides area-representative summaries while reducing the mixing of heterogeneous aquifer conditions relative to coarser aggregation units. This choice reflects that, at the global scale, aquifer boundaries and vertical structure cannot be delineated consistently from the available data in the CGWL dataset and existing global hydrogeologic datasets (Supplementary Information Section A2). We used H3-8 grid cells as the primary analysis unit, but repeated all key diagnostics on coastal HydroBASINS level-12 catchments (HYBAS-12; refs. 64,65) as a sensitivity test. Aggregation error, quantified as the root mean square error between well-level and unit-level median WTD, is lowest for H3-8 and increases for larger aggregation units, while it decreases primarily with the number of wells per unit. HYBAS-12 basins are on average ~141 km^2 (about four times larger than H3-6 hexagonal grid cells, ~36 km^2), yet the share of multiwell units is similar for HYBAS-12 and H3-6 and aggregation error is slightly larger for HYBAS-12, indicating no systematic reduction of aggregation error relative to grid-based schemes with comparable well support (Supplementary Information Section A3). We therefore assume that any discrepancies between H3-8 and HYBAS-12 primarily reflect aggregation and sampling effects, that is, how differently sized spatial units mix heterogeneous conditions and how unevenly well density weights regional summaries. Against this background, HYBAS-12 closely reproduces the H3-8 patterns across IPCC coastal regions and distance-to-coast bands for flat-gradient prevalence, trend activity (|slope| ≥ 0.1 m yr^{-1}), the fraction of downward trends among trend-active units and the share of persistent/emerging flat-gradient hotspots (Spearman ρ_s = 0.87–0.95). Global differences are small, although a few regions deviate by >10 percentage points; for example, grids yield higher flat-gradient prevalence in Western Europe (WCE), while HYBAS-12 shifts the Caribbean (CAR) towards more upward and fewer downward trends, resulting in fewer persistent/emerging hotspots (Supplementary Information Section B4).

Bottom-up approach and representativeness limits. Our analysis is global in extent but bottom-up, scaling local well observations to consistent spatial units and from there to regional and global SWI-susceptibility indicators. The spatial representativeness of these indicators, both geographically and with respect to hydrogeologic settings, is constrained by uneven data coverage globally and the limited hydrogeologic characterization (notably aquifer system architecture and confinement). Our chosen fine grid-based aggregation can overweight densely monitored coastal areas and may regionally yield slightly different hotspot and trend-activity shares than coarser units, but it reduces the mixing of heterogeneous aquifer conditions.

Simplifications with GWL-based indicators. While this study uses GWL-based indicators to assess SWI susceptibility, it necessarily simplifies the physical complexity of coastal aquifer systems, where

salinization can propagate through several interconnected pathways: over land (storm surge and tidal flooding), under land via groundwater transport and through natural and engineered surface-water networks and via vertical processes such as upconing of deeper saline water beneath pumping wells[15,66]. Our indicators do not explicitly represent salinity or density-driven flow, limited by salinity observations being far less available than GWL time series at large scales[67,68] and co-located water-quality and water-quantity records being uncommon[69]. The indicators also simplify temporal dynamics relevant to SWI. In particular, gradients often rely on a single or short snapshot of head data, which is insufficient to quantify variability or detect shifts, while monotonic trends summarize net change over the analysis window and may miss transient or nonlinear changes.

Trend robustness and record-length sensitivity. Since trend direction at individual locations can be sensitive to record length and to the timing of multiannual variability or management interventions, regions with spatiotemporally inconsistent trends require particularly careful interpretation. However, our 9- versus 19-year comparison indicates that, while longer records are generally more robust, 9-year time series already capture the qualitative direction of GWL change for most regions, with notable exceptions such as in southeastern Australia and India, where declines are stronger and more frequent in the more recent 9-year window. Multiwindow trend reporting can serve as a practical robustness check when long GWL records are unavailable.

Limits to causal inference and attribution. In general, this study does not establish causation. Because gridded population products redistribute census counts, population-based contrasts (and any future projections) carry spatially heterogeneous uncertainty. Specifically, they can systematically under-represent rural populations and misallocate density within cities[70,71]. Given the substantial uncertainties in both global recharge projections and pumping estimates when interpreted at the scale of local observations[51,62], we do not directly attribute the observed gradients and trends to these drivers (Fig. 4b,c). Instead, we use the AI as a proxy for recharge limitation and, indirectly, for potential future increases in water stress and demand. However, we acknowledge that its bicategorical application (like the gradient split) is a coarse simplification that facilitates transparent global screening, but can mask precipitation effects relevant to recharge and compress diverse hydroclimatic (and hydro-ecological) settings into broad classes[41,72].

Data availability

The CGWL dataset is publicly available via Zenodo at https://doi.org/10.5281/zenodo.15008065 (ref. 73) under a CC-BY-NC license, including all data sources obtained with permission for publishing or under open licences. Data for conducting trend and SWI-susceptibility analyses are also available via Zenodo at https://doi.org/10.5281/zenodo.16812560 (ref. 74). Additional datasets used in these analyses are referenced within the same repository.

Code availability

Code for conducting trend and SWI-susceptibility analyses is available via Zenodo at https://doi.org/10.5281/zenodo.16812560 (ref. 74).

References

1. Cosby, A. G. et al. Accelerating growth of human coastal populations at the global and continent levels: 2000–2018. *Sci. Rep.* **14**, 22489 (2024).
2. Dyring, M., Hofmann, H., Stanton, D., Moss, P. & Froend, R. Ecohydrology of coastal aquifers in humid environments and implications of a drying climate. *Ecohydrology* **16**, e2491 (2022).
3. Luijendijk, E., Gleeson, T. & Moosdorf, N. Fresh groundwater discharge insignificant for the world's oceans but important for coastal ecosystems. *Nat. Commun.* **11**, 1260 (2020).
4. Lecher, A. L. & Mackey, K. R. M. Synthesizing the effects of submarine groundwater discharge on marine biota. *Hydrology* **5**, 60 (2018).
5. Neumann, B., Vafeidis, A. T., Zimmermann, J. & Nicholls, R. J. Future coastal population growth and exposure to sea-level rise and coastal flooding—a global assessment. *PLoS ONE* **10**, e0118571 (2015).
6. Mueller, W. et al. Saltwater intrusion and human health risks for coastal populations under 2050 climate scenarios. *Sci. Rep.* **14**, 15881 (2024).
7. Ghirardelli, A. et al. Global impact of seawater intrusion on coastal agriculture. *Environ. Res. Lett.* **20**, 13005 (2024).
8. Tully, K. et al. The invisible flood: the chemistry, ecology, and social implications of coastal saltwater intrusion. *BioScience* **69**, 368–378 (2019).
9. Venâncio, C., Ribeiro, R. & Lopes, I. Seawater intrusion: an appraisal of taxa at most risk and safe salinity levels. *Biol. Rev.* **97**, 361–382 (2022).
10. IPCC. *Climate Change 2021: The Physical Science Basis* (eds Masson-Delmotte, V. et al.) (Cambridge Univ. Press, 2021).
11. Richardson, C. M. et al. The impacts of climate change on coastal groundwater. *Nat. Rev. Earth Environ.* **5**, 100–119 (2024).
12. Spinoni, J. et al. How will the progressive global increase of arid areas affect population and land-use in the 21st century?. *Global Planet. Change* **205**, 103597 (2021).
13. Kretschmer, D. V. et al. A perceptual model of drivers and limiters of coastal groundwater dynamics. *Hydrol. Process.* **39**, e70058 (2025b).
14. Werner, A. D. On the classification of seawater intrusion. *J. Hydrol.* **551**, 619–631 (2017).
15. Werner, A. D. et al. Vulnerability indicators of sea water intrusion. *Groundwater* **50**, 48–58 (2012).
16. Michael, H. A., Russoniello, C. J. & Byron, L. A. Global assessment of vulnerability to sea-level rise in topography-limited and recharge-limited coastal groundwater systems. *Water Resour. Res.* **49**, 2228–2240 (2013).
17. Cuthbert, M. O. et al. Global patterns and dynamics of climate–groundwater interactions. *Nat. Clim. Change* **9**, 137–141 (2019).
18. Fan, X., Peterson, T. J., Henley, B. J. & Arora, M. Groundwater sensitivity to climate variations across Australia. *Water Resources Research* **59**, e2023WR035036 (2023).
19. Gleeson, T., Cuthbert, M., Ferguson, G. & Perrone, D. Global groundwater sustainability, resources, and systems in the Anthropocene. *Annu. Rev. Earth Planet. Sci.* **48**, 431–463 (2020).
20. Costall, A. R. et al. Groundwater throughflow and seawater intrusion in high quality coastal aquifers. *Sci. Rep.* **10**, 9866 (2020).
21. Morgan, L. K. & Werner, A. D. A national inventory of seawater intrusion vulnerability for Australia. *J. Hydrol. Reg. Stud.* **4**, 686–698 (2015).
22. Gleeson, T. et al. GMD perspective: the quest to improve the evaluation of groundwater representation in continental- to global-scale models. *Geosci. Model Dev.* **14**, 7545–7571 (2021).
23. Adams, K. H. et al. Climate-induced saltwater intrusion in 2100: recharge-driven severity, sea level-driven prevalence. *Geophys. Res. Lett.* **51**, e2024GL110359 (2024).
24. Kretschmer, D. V. et al. Controls on coastal saline groundwater across North America. *Environ. Res. Lett.* **20**, 24065 (2025).
25. Zamrsky, D., Oude Essink, G. H. P. & Bierkens, M. F. P. Global impact of sea level rise on coastal fresh groundwater resources. *Earth's Future* **12**, e2023EF003581 (2024).
26. Reinecke, R. et al. Uncertainty in model estimates of global groundwater depth. *Environ. Res. Lett.* **19**, 114066 (2024).
27. Arifin, A. et al. Plausibility criteria for GRACE-derived groundwater storage changes from aquifers globally. *Geophys. Res. Lett.* **52**, e2025GL118580 (2025).

28. Costantini, M., Colin, J. & Decharme, B. Projected climate-driven changes of water table depth in the world's major groundwater basins. *Earth's Future* **11**, e2022EF003068 (2023).
29. Frappart, F. & Ramillien, G. Monitoring groundwater storage changes using the Gravity Recovery and Climate Experiment (GRACE) satellite mission: a review. *Remote Sens.* **10**, 829 (2018).
30. Ferguson, G. & Gleeson, T. Vulnerability of coastal aquifers to groundwater use and climate change. *Nat. Clim. Change* **2**, 342–345 (2012).
31. Jasechko, S., Perrone, D., Seybold, H., Fan, Y. & Kirchner, J. W. Groundwater level observations in 250,000 coastal US wells reveal scope of potential seawater intrusion. *Nat. Commun.* **11**, 3229 (2020).
32. Famiglietti, J. S. & Rodell, M. Water in the balance. *Science* **340**, 1300–1301 (2013).
33. Lall, U., Josset, L. & Russo, T. A snapshot of the world's groundwater challenges. *Annu. Rev. Environ. Resour.* **45**, 171–194 (2020).
34. *Groundwater—Making the Invisible Visible* (UN, 2022); https://doi.org/10.18356/9789210015363
35. Fan, Y., Li, H. & Miguez-Macho, G. Global patterns of groundwater table depth. *Science* **339**, 940–943 (2013).
36. Ma, Y. et al. Water table depth estimates over the contiguous United States using a random forest model. *Groundwater* **62**, 34–43 (2024).
37. Shokri-Kuehni, S. M. S. et al. Water table depth and soil salinization: from pore-scale processes to field-scale responses. *Water Resour. Res.* **56**, e2019WR026707 (2020).
38. Jasechko, S. et al. Rapid groundwater decline and some cases of recovery in aquifers globally. *Nature* **625**, 715–721 (2024).
39. Chávez García Silva, R. et al. Multi-decadal groundwater observations reveal surprisingly stable levels in southwestern Europe. *Commun. Earth Environ.* **5**, 387 (2024).
40. Nolte, A., Haaf, E., Heudorfer, B., Bender, S. & Hartmann, J. Disentangling coastal groundwater level dynamics in a global dataset. *Hydrol. Earth Syst. Sci.* **28**, 1215–1249 (2024).
41. Zomer, R. J., Xu, J. & Trabucco, A. Version 3 of the global aridity index and potential evapotranspiration database. *Sci. Data* **9**, 409 (2022).
42. Berghuijs, W. R. et al. Groundwater recharge is sensitive to changing long-term aridity. *Nat. Clim. Change* **14**, 357–363 (2024).
43. Iturbide, M. et al. An update of IPCC climate reference regions for subcontinental analysis of climate model data: definition and aggregated datasets. *Earth Syst. Sci. Data* **12**, 2959–2970 (2020).
44. Baulon, L. et al. Influence of low-frequency variability on groundwater level trends. *J. Hydrol.* **606**, 127436 (2022).
45. Kuss, A. J. M. & Gurdak, J. J. Groundwater level response in US principal aquifers to ENSO, NAO, PDO, and AMO. *J. Hydrol.* **519**, 1939–1952 (2014).
46. *Applying the Degree of Urbanisation: A Methodological Manual to Define Cities, Towns and Rural Areas for International Comparisons* (European Union, 2021).
47. Cao, T., Han, D. & Song, X. Past, present, and future of global seawater intrusion research: a bibliometric analysis. *J. Hydrol.* **603**, 126844 (2021).
48. Hamlington, B. D. et al. The rate of global sea level rise doubled during the past three decades. *Commun. Earth Environ.* **5**, 601 (2024).
49. Kopp, R. E. et al. Communicating future sea-level rise uncertainty and ambiguity to assessment users. *Nat. Clim. Change* **13**, 648–660 (2023).
50. Jakovovic, D., Werner, A. D. & Simmons, C. T. Numerical modelling of saltwater up-coning: comparison with experimental laboratory observations. *J. Hydrol.* **402**, 261–273 (2011).
51. Nazari, S., Reinecke, R. & Moosdorf, N. Global estimates of groundwater withdrawal trends and uncertainties. *Environ. Res. Lett.* **20**, 94043 (2025).
52. Ravinandrasana, V. P. & Le Franzke, C. The first emergence of unprecedented global water scarcity in the Anthropocene. *Nat. Commun.* **16**, 8281 (2025).
53. Nolte, A. et al. Hydrological modelling for assessing spatio-temporal groundwater recharge variations in the water-stressed Amathole Water Supply System, Eastern Cape, South Africa. *Hydrol. Process.* **35**, e14264 (2021).
54. Kulp, S. A. & Strauss, B. H. New elevation data triple estimates of global vulnerability to sea-level rise and coastal flooding. *Nat. Commun.* **10**, 4844 (2019).
55. *NASADEM Merged DEM Global 1 arc second V001* (LP DAAC, 2020); https://doi.org/10.5067/MEASURES/NASADEM/NASADEM_HGT.001
56. *H3: Hexagonal Hierarchical Geospatial Indexing System* (Uber Technologies, 2024); https://h3geo.org/
57. Sayre, R. et al. A global ecological classification of coastal segment units to complement marine biodiversity observation network assessments. *Oceanography* **34**, 120–129 (2021).
58. Yue, S. & Wang, C. The Mann–Kendall test modified by effective sample size to detect trend in serially correlated hydrological series. *Water Resour. Manag.* **18**, 201–218 (2004).
59. Sen, P. K. Estimates of the regression coefficient based on Kendall's tau. *J. Am. Stat. Assoc.* **63**, 1379–1389 (1968).
60. Trabucco, A. & Zomer, R. J. Global aridity index and potential evapotranspiration (et0) database: version 3. *figshare* https://doi.org/10.6084/m9.figshare.7504448.v5 (2022).
61. Nazari, S., Reinecke, R. & Moosdorf, N. Global sectoral groundwater withdrawal: estimates and uncertainty analysis. *PANGAEA* https://doi.org/10.1594/PANGAEA.982842 (2025).
62. Reinecke, R. et al. Uncertainty of simulated groundwater recharge at different global warming levels: a global-scale multi-model ensemble study. *Hydrol. Earth Syst. Sci.* **25**, 787–810 (2021).
63. *Gridded Population of the World, Version 4 (GPWv4): Population Density, Revision 11 (Version 4.11)* (NASA SEDAC, 2018); https://doi.org/10.7927/H49C6VHW
64. Lehner, B. *HydroBASINS: Global Watershed Boundaries and Sub-basin Delineations Derived From Hydrosheds Data at 15 Second Resolution: Technical Documentation Version 1.c* (HydroSheds, 2014); https://hydrosheds.org/page/hydrobasins
65. Lehner, B. & Grill, G. Global river hydrography and network routing: baseline data and new approaches to study the world's large river systems. *Hydrol. Process.* **27**, 2171–2186 (2013).
66. Helton, A. M. et al. Over, under, and through: hydrologic connectivity and the future of coastal landscape salinization. *Water Resour. Res.* **61**, e2024WR038720 (2025).
67. Panthi, J., Pradhanang, S. M., Nolte, A. & Boving, T. B. Saltwater intrusion into coastal aquifers in the contiguous United States—a systematic review of investigation approaches and monitoring networks. *Sci. Total Environ.* **836**, 155641 (2022).
68. Thorslund, J. & van Vliet, M. T. H. A global dataset of surface water and groundwater salinity measurements from 1980–2019. *Sci. Data* **7**, 231 (2020).
69. Ebeling, P. et al. Water quality, discharge and catchment attributes for large-sample studies in Germany—QUADICA. *Earth Syst. Sci. Data* **14**, 3715–3741 (2022).
70. Kuffer, M., Owusu, M., Oliveira, L., Sliuzas, R. & van Rijn, F. The missing millions in maps: exploring causes of uncertainties in global gridded population datasets. *ISPRS Int. J. Geo-Inf.* **11**, 403 (2022).
71. Láng-Ritter, J., Keskinen, M. & Tenkanen, H. Global gridded population datasets systematically underrepresent rural population. *Nat. Commun.* **16**, 2170 (2025).

72. Taylor, R. G. et al. Ground water and climate change. *Nat. Clim. Change* **3**, 322–329 (2013).
73. Nolte, A. Coastal groundwater level (CGWL) dataset. *Zenodo* https://doi.org/10.5281/zenodo.15008065 (2026).
74. Nolte, A. et al. Coastal groundwater level trends reveal global susceptibility to seawater intrusion—code & data. *Zenodo* https://doi.org/10.5281/zenodo.16812560 (2026).
75. Iturbide, M. et al. SantanderMetGroup/ATLAS: final version of "IPCC WGI reference regions v4". *Zenodo* https://doi.org/10.5281/zenodo.3998463 (2020).

Acknowledgements

We would like to thank all the governmental agencies listed in Supplementary Information Section A for supporting this work by providing groundwater data and being available to answer questions about the data. This work was financed in the framework of the Helmholtz Institute for Climate Service Science (HICSS), a cooperation between the Climate Service Center Germany (GERICS) and Universität Hamburg, Germany, and conducted as part of the Future-H2O (Future climate and land-use change impacts on groundwater recharge rates and water quality for water resources) project.

Author contributions

Conceptualization: A.N. and R.R. Data curation: A.N. Formal analysis: A.N. and R.R. Funding acquisition: S. Bender and J.H. Investigation: A.N. Methodology: A.N., S. Baltruschat, N.M. and R.R. Supervision: S. Bender and J.H. Writing—original draft: A.N. and R.R. Writing—review and editing: A.N., S. Bender, J.H., S. Baltruschat, N.M. and R.R.

Funding

Open access funding provided by Universität Hamburg.

Competing interests

The authors declare no competing interests.

Additional information

Supplementary information The online version contains supplementary material available at https://doi.org/10.1038/s44221-026-00619-8.

Correspondence and requests for materials should be addressed to Annika Nolte.

Peer review information *Nature Water* thanks Daniel Gonzalez-Duque and the other, anonymous, reviewer(s) for their contribution to the peer review of this work. Peer reviewer reports are available.